# Photoinduced bond cleavage in $CH_3ReO_3$: excited state dynamics

**Paulo Jorge Costa,*[a] Maria José Calhorda,[a] Sébastien Villaume[b] and Chantal Daniel*[b]**

***Received (in Montpellier, France) 14th January 2008, Accepted 3rd June 2008***
***First published as an Advance Article on the web 6th August 2008***
**DOI: 10.1039/b800585k**

The rhenium–methyl bond cleavage in $CH_3ReO_3$ has been investigated by means of quantum chemical calculations of the one-D potential energy surfaces (PES) associated to the low-lying singlet and triplet excited states of the molecule. The quantum dynamics is studied by wave packet propagations on the b $^1A_1$ absorbing state coupled non-adiabatically to the low-lying a $^1E$ state. The spin–orbit states and spin–orbit couplings are evaluated according to the zeroth-order regular approximation (ZORA). The spin–orbit coupling between the a $^1E$ state and the a $^3A_1$ dissociative state controls the radical formation $^\bullet CH_3$ + $^\bullet ReO_3$, which occurs in 400 fs.



## Introduction

Among many oxide derivatives, methyltrioxorhenium (MTO), $CH_3ReO_3$, has been the object of a number of experimental and theoretical studies.[1] This molecule is a remarkable catalyst for a large number of reactions such as olefin metathesis, oxidation and aldehyde olefination, for instance.[2] MTO displays different photochemical behavior upon irradiation in solution[3] and in low-temperature matrices.[4] Indeed, whereas a carbene tautomer is observed in frozen matrix, the rhenium–methyl bond homolysis is the primary reaction observed in solution, leading to radicals $^\bullet ReO_3$ and $^\bullet CH_3$ (eqn (1)).

$$CH_3ReO_3 \xrightarrow{260\ nm} {}^\bullet CH_3 + {}^\bullet ReO_3 \qquad (1)$$

Despite the number of studies performed on this class of molecules, little is known on the excited states reactivity and associated photochemical mechanism. In a recent work,[5] we have revisited the photochemistry of MTO by means of TD-DFT and CASSCF/MS-CASPT2 methods. The electronic structure has been re-analyzed in order to assign the electronic transitions and to propose a qualitative mechanism describing the homolysis of the methyl–rhenium bond after irradiation at 260 nm. The lowest allowed $^1A_1$ transition, calculated at 257 nm (CASCF/MS-CASPT2), corresponds to a charge transfer from the oxygen lone pairs ($p_O$) to a metal centered orbital ($\pi^*_{Re-O}$) in agreement with TD-DFT results, showing that the previous semi-empirical assignment of this state as a $\sigma_{Re-C} \rightarrow \pi^*_{Re-O}$ was incorrect.[3] The next transitions, calculated at 240 and 231 nm, correspond to charge transfer from C and O to Re. Analogous compounds were also investigated, such as $(C_2H_5)ReO_3$ with a very similar theoretical absorption spectrum or $(C_6H_5)ReO_3$ and $\{C_6H_3(CH_3)_3\}ReO_3$ characterized by a strong low absorption dominated by a ligand to metal charge transfer from the $\pi^*_{phenyl}$ to $d_{Re}$ ($\pi^*_{Re-O}$).

Herein we report the one-dimensional CASSCF potential energy curves associated to the low-lying singlet and triplet excited states of $CH_3ReO_3$ and computed for the rhenium–methyl bond homolysis $q_a$ = [Re–$CH_3$] coordinate. The quantum chemical calculations are supplemented by wave packet propagations in order to simulate the main features of the electronic absorption spectrum and the dynamics of the homolysis.

## Results and discussion

### Franck–Condon transitions—spin–orbit effect

The spin-free and spin–orbit states of $CH_3ReO_3$ and corresponding transition energies and oscillator strengths are reported in Table 1. In agreement with our previous study[5] the b $^1A_1$ state calculated at 262 nm (TD-DFT) is the best candidate for direct absorption from the a $^1A$ electronic ground state. A second singlet state with significant oscillator strength, namely the b $^1E$ (266 nm, TD-DFT) could also play a role at the early stage of the dynamics.

In order to estimate the spin–orbit couplings between the low-lying singlet and triplet states of $CH_3ReO_3$, nine spin-free states of $A_1$, E and $A_2$ symmetries have been included. This generates seventeen spin–orbit states of $A_1$, $A_2$ and E symmetries.

The absorption spectrum is broadened by spin–orbit effects and intensity is lowered. These general trends have been observed in previous theoretical studies on various transition metal complexes.[6] The spin–orbit splitting of most of the spin-free states amounts to 1000 $cm^{-1}$ or more. If we exclude the a $^3E$ state which remains nearly pure, most of the spin–orbit states originate from significant contributions of several spin-free states. Surprisingly, the spin–orbit effects on the transition energies are not significant at this level of approximation (ZORA) and the theoretical absorption spectrum is not drastically shifted, except for the b $^1E$ state where a significant shift ($\sim$4400 $cm^{-1}$) is calculated with a decrease of the oscillator strength. This red shift is due to the important contribution of the a $^3A_1$ and a $^3A_2$ states

[a] *Departamento de Química e Bioquímica, CQB, Faculdade de Ciências da Universidade de Lisboa, 1749-016 Lisboa, Portugal. E-mail: pjcosta@fc.ul.pt*
[b] *Laboratoire de Chimie Quantique, UMR 7177 CNRS, Université Louis Pasteur, Institut Le Bel, 4, rue Blaise Pascal, 67000 Strasbourg, France. E-mail: daniel@quantix.u-strasbg.fr*

 

**Table 1** TD-DFT transition energies to the lowest spin-free and spin–orbit electronic states of $CH_3ReO_3$ and associated oscillator strengths

| State | $E$/cm$^{-1}$ | $E$/nm | $f$ | SO states | $E$/cm$^{-1}$ | $f$ |
|---|---|---|---|---|---|---|
| a $^3$E | 31 938 | 313 | 0.0 | $A_1$ (98% a $^3$E) | 31 196 | 0.0 |
| | | | | $A_2$ (99% a $^3$E) | 31 203 | 0.0 |
| | | | | E (87% a $^3$E) | 32 461 | 0.0 |
| b $^3$E | 33 745 | 296 | 0.0 | $A_2$ (67% b $^3$E, 24% a $^3A_1$) | 33 094 | 0.0 |
| | | | | $A_1$ (83% b $^3$E, 11% a $^3A_2$) | 33 321 | 0.0003 |
| | | | | E (46 % b $^3$E, 21% c $^3$E, 15% b $^1$E) | 33 638 | 0.0 |
| a $^3A_1$ | 34 254 | 292 | 0.0 | $A_2$ (64% a $^3A_1$, 30% b $^3$E) | 34 324 | 0.0 |
| | | | | E (46% a $^3A_1$, 30% a $^3A_2$) | 35 429 | 0.0003 |
| a $^3A_2$ | 34 795 | 287 | 0.0 | E (40% a $^3A_2$, 21% b $^1$E, 19% a $^3A_1$) | 32 998 | 0.0 |
| | | | | $A_1$ (73% a $^3A_2$, 14% b $^3$E, 11% c $^3$E) | 34 625 | 0.0001 |
| a $^1$E | 35 060 | 285 | 0.0025 | E (47% a $^3$E, 41% a $^1$E) | 35 079 | 0.0016 |
| c $^3$E | 36 985 | 270 | 0.0 | $A_2$ (64% c $^3$E, 24% a $^1A_2$) | 36 180 | 0.0 |
| | | | | $A_1$ (71% c $^3$E, 14% a $^3A_2$, 13% b $^1A_1$) | 36 442 | 0.0012 |
| | | | | E (35% c $^3$E, 26% c $^1$E, 16% b $^3$E) | 37 419 | 0.0 |
| a $^1A_2$ | 37 309 | 268 | 0.0 | $A_2$ (73% a $^1A_2$, 24% c $^3$E) | 37 656 | 0.0 |
| b $^1$E | 37 527 | 266 | 0.0036 | E (29% b $^1$E, 21% a $^3A_1$, 19% a $^3A_2$) | 33 156 | 0.0001 |
| b $^1A_1$ | 38 079 | 262 | 0.0054 | $A_1$ (84% b $^1A_1$, 13% c $^3$E) | 38 215 | 0.0031 |

**Table 2** Calculated CASSCF transition energies (cm$^{-1}$ and nm) of $CH_3ReO_3$ and associated oscillator strengths compared with experimental values ($\lambda_{exp}$)

| State | $E$/cm$^{-1}$ | $E$/nm | $f$ | $\lambda_{exp}$/nm |
|---|---|---|---|---|
| a $^1$E | 33 222 | 301 | 0.0003 | |
| **b $^1A_1$** | **39 370** | **254** | **0.0067** | **260** |
| b $^1$E | 43 478 | 230 | 0.0061 | 231 |
| c $^1$E | 53 191 | 188 | 0.0361 | 205 |

calculated at 34 254 and 34 795 cm$^{-1}$, respectively. They contribute by 40% to the spin-orbit SO E state, as compared to the 29% contribution of the b $^1$E state. However, the impact of these changes on the calculated spectra should be minimal since the observed band at 260 nm is attributed to the b $^1A_1$ state.

The CASSCF and the TD-DFT results, reported in Table 2 and Table 1, respectively, qualitatively agree with the assignment of the b $^1A_1$ as the absorbing state. The relative order of b $^1$A and b $^1$E, very close in energy at the TD-DFT level, is reversed by CASSCF calculations with only one excited state calculated at 301 nm (a $^1$E) below the b $^1A_1$ absorbing state.

Above b $^1A_1$, we enter the region of the second observed band in the experimental UV-Vis spectra. Therefore, for the simulation, only the a $^1$E and b $^1A_1$ CASSCF calculated states were considered (*vide infra*). These CASSCF results agree with the previously reported MS-CASPT2 results.[5]

## Potential energy surfaces

The adiabatic CASSCF potential energy surfaces (PES) associated to the low-lying singlet and triplet electronic states of $CH_3ReO_3$ are depicted in Fig. 1. The singlet absorbing states assigned to ligand-to-metal-charge-transfer (LMCT) states corresponding mainly to $p_O \rightarrow d_{Re}(\pi^*_{Re-O})$ or $p_O$, $p_C \rightarrow d_{Re}(\pi^*_{Re-O})$ excitations[5] are bound with respect to the metal–methyl bond elongation. The shape of the singlet PES rules out a direct ultra-fast (fs) homolysis of the metal–methyl bond under irradiation at 254 nm. After absorption the system should be trapped into the potential well of the lowest states. The photoreactivity will be governed by longer time-scale intersystem crossing processes towards the low-lying triplet states.

The triplet PES represented in Fig. 1(b) exhibit complicated profiles with a number of avoided crossings and energy barriers. The upper states are bound with respect to the metal–methyl bond homolysis. The only dissociative state is the a $^3A_1$ corresponding to the $\sigma_{Re-CH_3} \rightarrow \sigma^*_{Re-CH_3}$ excitation leading to the formation of the diradical primary products $^\bullet ReO_3 + {}^\bullet CH_3$ in the degenerate singlet and triplet states. Due to its high energy at the equilibrium this state generates several avoided crossings with the other triplet states.

The main consequence is the presence of an energy barrier, calculated at 4000 cm$^{-1}$ at about 2.7 Å, with a dramatic effect on the dissociative mechanism.

The efficiency of the metal–methyl bond homolysis will depend on the spin–orbit coupling between the singlet

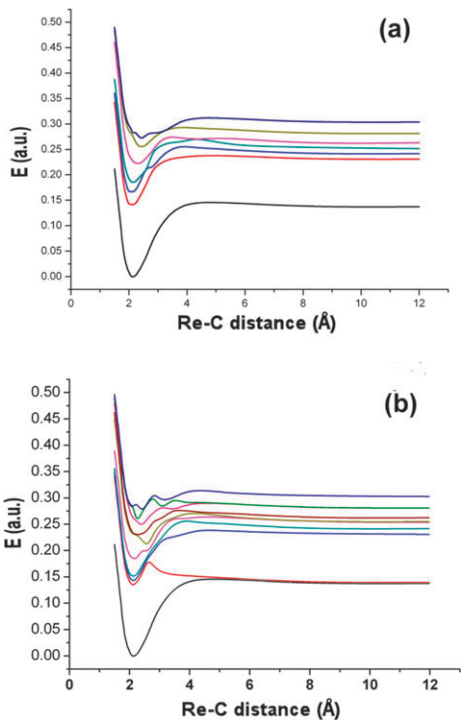


**Fig. 1** CASSCF PES associated to the low-lying singlet (a) and triplet (b) states $CH_3ReO_3$ as a function of the [Re–$CH_3$] distance ($q_a$).

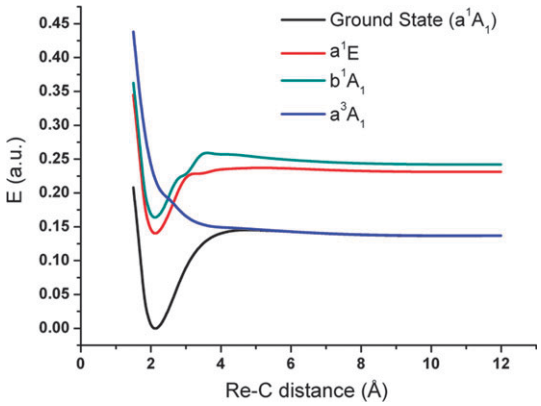


**Fig. 2** Selected PES (a $^1A_1$, b $^1A_1$, a $^3A_1$, a $^1E$) used for the simulation of the photodissociation of MTO.

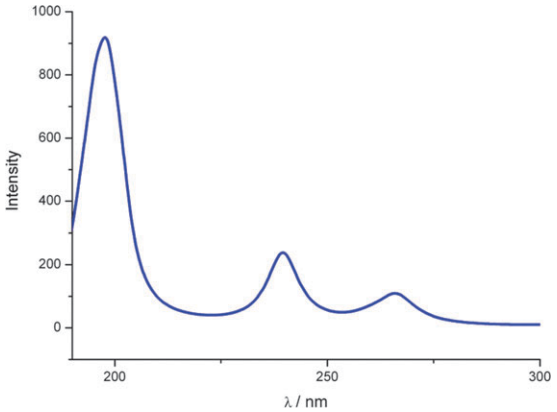


**Fig. 3** Simulated absorption spectrum of MTO.

absorbing states a $^1E$ and b $^1A_1$ (E spin–orbit state; $A_1$ spin–orbit state) and this low-lying triplet state a $^3A_1$ ($A_2$ + 2E spin–orbit states) and on the position of the crossing between them with respect to this energy barrier. Despite the complexity of the PES depicted in Fig. 1, selected states can be extracted to perform quantum dynamics simulations.

In order to build the electronic absorption spectrum, wave packet propagations were performed on the set of singlet PES depicted in Fig. 1(a). In a second set of simulations of the photodissociation of $CH_3ReO_3$, the electronic ground state, the a $^1A_1$ and a $^1E$ singlet states and the diabatic a $^3A_1$ dissociative state were selected (Fig. 2). In this qualitative approach, the PES have not been recalculated including spin–orbit effect. The simulation is performed within the quasi-diabatic approximation[7,8] taking into account the fact that the a $^3A_1$ PES, which should be split into two E and one $A_2$ components (see Table 1) is coupled with the b $^1E$ *via* the E component.

### Electronic absorption spectra

The simulated absorption spectrum of $CH_3ReO_3$ is depicted in Fig. 3. This spectrum has been obtained by propagation of selected wave packets on the singlet PES represented in Fig. 1. It is characterized by three absorption bands, namely, one intense peak and two weaker ones with maxima at 205, 235 and 260 nm, respectively. This spectrum compares rather well with the experimental electronic spectrum of MTO in *n*-hexane, which consists of three absorption bands with maxima at 205, 231 and 260 nm.[3] This good agreement validates *a posteriori* the shape of the singlet PES fitted over the 18 CASSCF *ab initio* points and allows further investigation of the dissociative mechanism by wave packets propagation on selected singlet/triplet PES coupled by spin–orbit.

### Photodissociation dynamics

In a first simulation, wave packet propagations have been performed on the PES represented in Fig. 2, where the minima of the electronic ground state and excited states coincide, according to the *ab initio* results. Several sets of simulations, with various spin–orbit coupling (SOC) values (from 500 to 5000 cm$^{-1}$) led to a non-dissociative process with oscillatory exchanges of populations between the singlet states, the wave packet being trapped in the minima of the a $^1E$ and b $^1A_1$ (see Fig. 4, left).

In a second approach, the PES of the electronic excited states (b $^1A_1$ and a $^1E$) have been shifted by $\delta q_a$ = 0.2 Å with respect to the electronic ground state potential. Indeed, in this simple 1-D scheme other vibrational relaxation effects are not taken into account. This qualitative approach allows us to control the kinetic energy of the wave packet when it comes close to the singlet–triplet crossing and to investigate its ability to populate efficiently the dissociative potential whatever the SOC is (from 500 to 5000 cm$^{-1}$). This is schematically illustrated in Fig. 4, right.

Snapshots of the wave packets simulating the photodissociation of $CH_3ReO_3$ after irradiation into the shifted b $^1A_1$ and a $^1E$ curves are represented in Fig. 5 for selected time scales and a SOC value of 1000 cm$^{-1}$. At the initial time ($t$ = 0 fs) both singlet states are populated. At 20 fs the upper a $^3A_1$ state is already significantly populated, whereas one major part of the wave packet is trapped into the potential well of the b $^1A_1$ state. As soon as the a $^3A_1$ dissociative state is populated, ultra-fast breaking of the Re–C bond is observed. Within 400 fs, 20% of the molecule dissociates towards $^\bullet ReO_3$ and $^\bullet CH_3$. Beyond this time-scale the simulation is not valid anymore due to the limited number of degrees of freedom taken into account.

The reactivity model described above also does not take into account solvent effects. It has been shown that the MTO

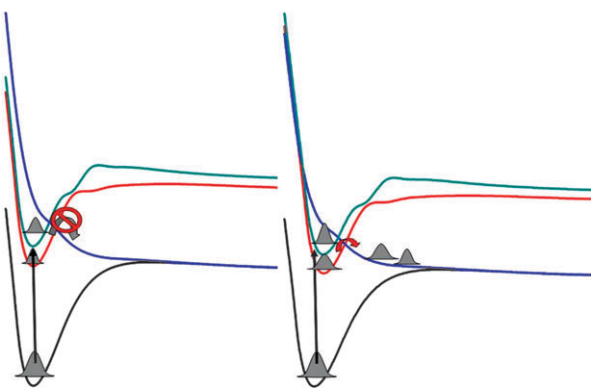

**Fig. 4** Schematic Frank–Condon population depending on the relative position of the potential: no shift (left) and 0.2 Å shift (right).

 

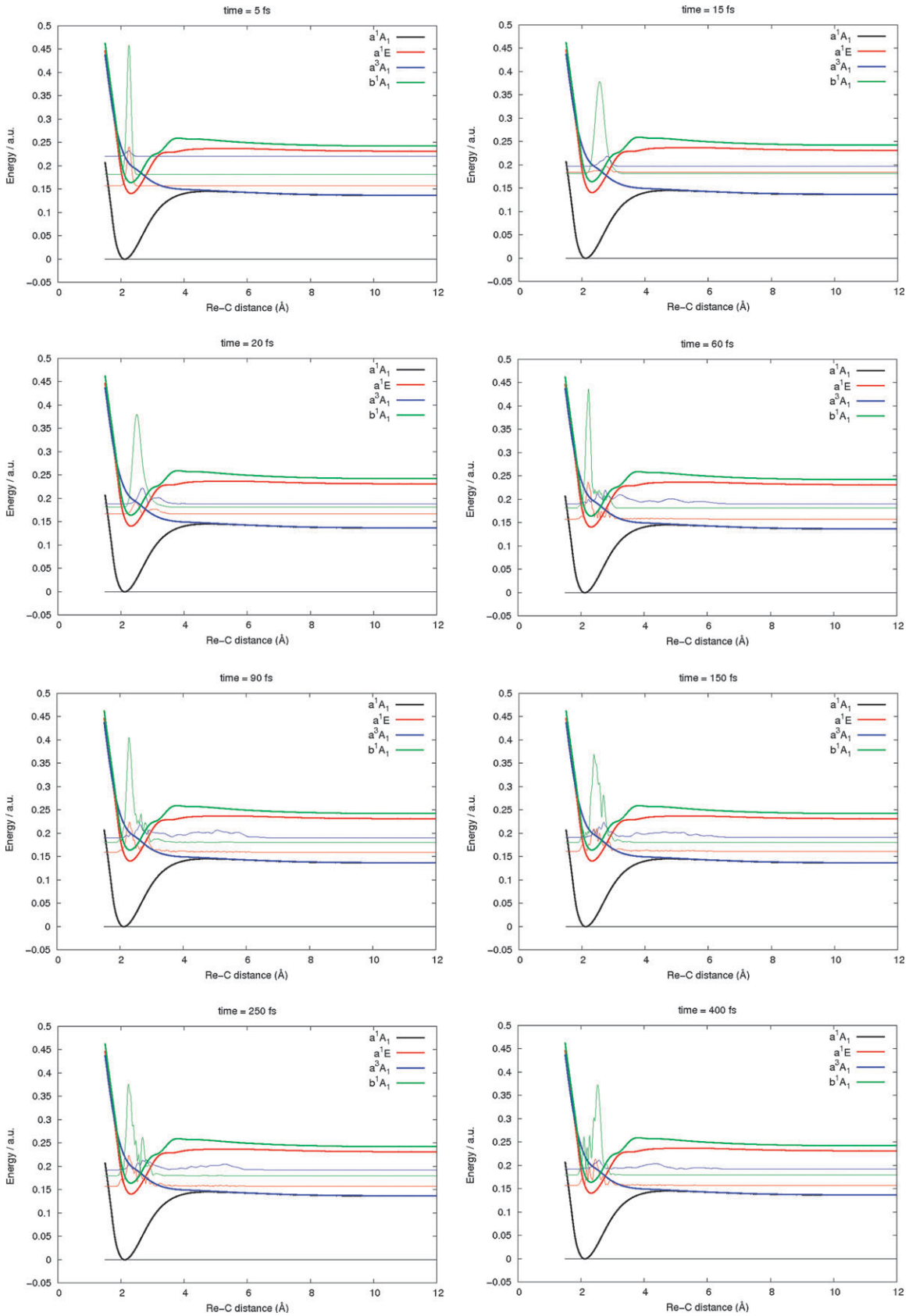


**Fig. 5** Snapshots of the simulated photodissociation of $CH_3ReO_3$ after irradiation into the shifted $a\,^1E$ and $b\,^1A_1$ potentials. Potential energy surfaces are represented in bold lines while the wave packets moving on each PES are represented with thin lines.

absorption spectrum is slightly dependent of the solvent,[3] and that photoreactivity apparently changes on going from solution to a frozen matrix.[4] However, our previous TD-DFT calculations have also shown that the impact of solvent effects in the calculated energy of the excited states is minimum.[5] Therefore, these gas-phase results should also contribute to a reliable qualitative model for the solution reactivity. Additionally, our calculations can provide some hints about the reactivity in a frozen matrix as reported by Downs and co-workers,[4] where the formation of the methylidene tautomer $H_2C{=}Re(O)_2OH$ is observed. Since our calculations refer to a single isolated MTO molecule, our reactivity model confirms the idea that this tautomer should be formed through a mechanism involving the homolysis of the Re–$CH_3$ bond in a first step, with subsequent rearrangement of the radicals in the frozen matrix. As suggested,[4b] the different reactivity should be just a reflex of the final fate of the radicals: in a frozen matrix they can interact and rearrange; in solution they can diffuse away from each other and interact with the solvent molecules.

## Conclusions

The TD-DFT spin–orbit absorption spectrum of MTO has been calculated within the ZORA approximation on the basis of nine low-lying spin-free states and seventeen spin–orbit states. The spin–orbit effects are of little influence on the shape and energetics of the theoretical spectrum between 260 and 310 nm. Three bands are detected with maxima at 205, 231 and 260 nm. The spin–orbit splitting of the spin-free states amounts to $\sim$1000–1500 $cm^{-1}$ and, at the TD-DFT level of theory, the calculated b $^1A_1$ state should contribute mainly to the observed band at 260 nm. At the CASSCF level of theory, two low-energy states (a $^1E$ and b $^1A_1$) are calculated at 301 and 254 nm, respectively. These states contribute to the photoreactivity of the complex, namely the metal–methyl bond homolysis observed in solution after irradiation at 260 nm. Simulation of the photodissociation dynamics by wave packet propagation on the coupled potentials, associated to the electronic ground state, calculated at the CASSCF level of theory to two singlet states (a $^1E$ and a $^1A_1$) and to the a $^3A_1$ ($\sigma_{Re-C}\sigma^*_{Re-C}$) dissociative state for the observed reaction, indicates that the a $^1E$ and a $^3A_1$ states are populated within the first tens of fs after absorption to the b $^1A_1$ state. The SO is activated *via* the E components of the spin–orbit states generated by the SOC splitting of the a $^1E$ and a $^3A_1$ spin-free states. Within the limit of our model (a 1-D simulation along the reactive coordinate corresponding to the Re–$CH_3$ bond elongation, considering only three excited states and an empirical shift of the potentials), 20% of the molecule dissociates in 400 fs, the rest of the system being trapped in the potential wells of the two singlet states. These results are dependent on the model used but can be applied qualitatively. On the basis of several simulations, it is shown that the efficiency of the singlet–triplet intersystem crossing does not depend only on the SOC values but also drastically on the available kinetic energy of the wave packet (induced by the potential shifts) when approaching the singlet–triplet crossing. Further work should be devoted to a refinement of the PES by performing more accurate *ab initio* calculations[9] and to an improvement of our model by including other nuclear relaxation effects in the electronic excited states.[10] Despite the complexity of the electronic problem, we have shown that the photoreactivity of MTO at the early stage (before 0.5 ps) is governed by the dynamics of only three excited states, the b $^1A_1$ absorbing state, the near a $^1E$ state (both bound and corresponding to excitation from the $p_O$ oxygen lone pairs to a $\pi^*_{ReO}$ metal centred orbital), and the a $^3A_1$ dissociative state.

## Computational details

The CASSCF calculations have been performed on the previously reported DFT/PW91 optimized geometry[5] under $C_{3v}$ symmetry constraints with MOLCAS,[11] with the following basis sets: the Re atom was described by the Dolg ECP ($Z$ = 15.0) with an associated (8s, 7p, 6d) valence basis set[12] whereas the atomic natural orbitals ANO[13] were used for the C, O and H atoms in the all-electron scheme with a (10s, 6p, 3d) set contracted to [4s, 3p, 2d] for C and O and a (7s, 3p) set contracted to [3s, 2p] for H. The potential energy curves (PES), associated to the seven low-lying singlet and six low-lying triplet states, have been calculated at the complete active space SCF level (CASSCF) using 14 electrons correlated in 10 active orbitals CAS(14,10), as a function of the $q_a$ bond elongation. The rest of the molecule was frozen in this 1-D approximation, already used in other applications.[8,14] It is justified by the fact that the $^1A_1$ ($p_O \rightarrow d_{Re}$) absorbing state should not be affected by other nuclear relaxation, such as the umbrella motion of the three oxygens. However, according to preliminary investigation of the relaxation effects during the course of the breaking of the Re–$CH_3$ bond, this nuclear coordinate should be considered in a further study. Indeed, DFT/PW91 geometry optimization of the fragment $ReO_3$ leads to a planar structure. The spin–orbit states and spin–orbit couplings have been evaluated within the ZORA approximation as implemented in the ADF package.[15]

The environment effects (solvent or matrix) have not been taken into account in this theoretical study, which aims at deciphering the mechanism of the photoinduced bond homolysis in the title complex. Obviously, this is a first step toward a more realistic model, which would take into account solvent effects by recomputing PES with an extra solvation coordinate. This approach is beyond the scope of the present work.

The simulation of the phodissociation dynamics is based on wave packet propagations on the PES, solving a set of coupled (either non-adiabatically or by spin–orbit) time dependent Schrödinger equation,

$$i\hbar\frac{\partial}{\partial t}|\phi_i(q_a,t)\rangle = \sum_j \hat{H}_{ij}(q_a)|\phi_j(q_a,t)\rangle \qquad (2)$$

where $\hat{H}_{ij}$ is the total Hamiltonian composed of the kinetic operator and of the PES $V_i(q_a)$. The kinetic energy operator defining the dissociation of $CH_3$, in a reduced one-dimensional model is given by

$$\hat{T} = \frac{\hbar}{2m}\frac{\partial^2}{\partial q_a^2} \qquad (3)$$

where $m$ is the reduced mass.

 

$$m = \frac{m_{CH_3} m_{ReO_3}}{m_{CH_3} + m_{ReO_3}} \quad (4)$$

$\Phi_f(q_a,t)$ are the time-dependent wave packets moving on $V_i(q_a)$. Following Heller,[16] the absorption spectrum has been calculated by means of a time-dependent approach. The total absorption spectrum is then calculated as Fourier transformation of the time-dependent total autocorrelation function $S_{tot}(t)$,

$$\sigma(\omega) \propto \int_{-\infty}^{+\infty} dt\, S_{tot}(t) \cdot \exp(i(E_0 + \hbar\omega)t/\hbar) \quad (5)$$

where $E_0$ is the energy of the vibrational ground state of the electronic ground state, and $\hbar\omega$ is the energy of the absorbed photon. The total autocorrelation function is the sum over the individual autocorrelation functions corresponding to each electronically excited state $I$

$$S_{tot}(t) = \sum_i S_i(t) = \sum_i \langle \phi_i(q_a, t=0 | \phi_i(q_a, t) \rangle \quad (6)$$

and describes the evolution of the molecular system in the electronically excited state $i$ by tracking the overlap of the wave function $\Phi_i(q_a,t)$ with the initial wave function $\Phi_i(q_a, t = 0)$ as a function of time $t$. The initial wave function is calculated as

$$\Phi_i(q_a;\ t\ =\ 0)\ =\ \tilde{\mu}_{fi}\varphi_0(q_a) \quad (7)$$

that is, we demand that the wave packet, as it starts in the upper electronic state $i$, equals the wave function of the vibrational ground state $\phi_0(q_a)$ multiplied by the normalized transition dipole function defined as

$$\tilde{\mu}_{fi} \equiv \tilde{\mu}_{f0} = \frac{\sqrt{\mu_{f0,x}^2 + \mu_{f0,y}^2 + \mu_{f0,z}^2}}{\sum_f \mu_{f0}} \quad (8)$$

The vibrational eigenstate $\phi_0(q_a)$ is evaluated using the Fourier transform grid Hamiltonian method.[17] The time-dependent propagation of the wave function is carried out in a grid of 1024 grid points based on *ab initio* eigenvalues, using the Chebychev propagator[18] as implemented in the Wavepacket 2 set of programs,[19] with a time step of 5 fs during 500 fs. In order to avoid unphysical reflections of the functions, an absorbing boundary potential[20] has been fixed at 6 Å in $q_a$. In some simulations the electronic excited potentials have been shifted with respect to the electronic ground state potential by 0.2 Å.



## Acknowledgements

P. J. C. thanks FCT for a grant (SFRH/BD/10535/2002). M. J. C. and P. J. C. thank FCT for financial support (project POCI/QUI/58925/2004). The authors gratefully acknowledge GRICES/FCT and CNRS (Programa Pessoa).

## References

1 (*a*) C. C Romão, F. E. Kühn and W. A. Herrmann, *Chem. Rev.*, 1997, **97**, 3197; (*b*) W. A. Herrmann, *J. Organomet. Chem.*, 1995, **500**, 149; (*c*) C. di Valentin, R. Gandolfi, P. Gisdakis and N. J. Rösch, *J. Am. Chem. Soc.*, 2001, **123**, 2365; (*d*) C. Mealli, J. A. López, M. J. Calhorda, C. C. Romão and W. A. Herrmann, *Inorg. Chem.*, 1994, **33**, 1139.
2 (*a*) F. E. Kühn, A. Scherbaum and W. A. Herrmann, *J. Organomet. Chem.*, 2004, **689**, 4149; (*b*) J. Jacob, J. H. Espenson, J. H. Jensen and M. S. Gordon, *Organometallics*, 1998, **17**, 1835.
3 H. Kunkeley, T. Türk, C. Teixeira, C. M. de Bellefon, W. A. Herrmann and A. Vogler, *Organometallics*, 1991, **10**, 2090.
4 (*a*) L. J. Morris, A. J. Downs, T. M. Greene, G. S. McGrady, W. A. Herrmann, P. Sirsch, O. Gropen and W. Scherer, *Chem. Commun.*, 2000, 67; (*b*) L. J. Morris, A. J. Downs, T. M. Greene and G. S. McGrady, *Organometallics*, 2001, **20**, 2344.
5 P. J. Costa, M. J. Calhorda, J. Bossert, C. Daniel and C. C. Romão, *Organometallics*, 2006, **25**, 5235.
6 V. Vallet, A. Strich and C. Daniel, *Chem. Phys.*, 2005, **33**, 13.
7 M. C. Heitz, C. Ribbing and C. Daniel, *J. Chem. Phys.*, 1997, **106**, 1421.
8 C. Daniel, D. Guillaumont, C. Ribbing and B. Minaev, *J. Phys. Chem. A*, 1999, **103**, 5765.
9 N. Ben Amor, D. Ambrosek, C. Daniel and R. Marquardt, *Chem. Phys.*, 2007, **338**, 81.
10 M. R. Brill, F. Gatti, D. Lauvergnat and H. D. Meyer, *Chem. Phys.*, 2007, **338**, 186.
11 G. Karlström, R. Lindh, P.-Å. Malmqvist, B. O. Roos, U. Ryde, V. Veryazov, P.-O. Widmark, M. Cossi, B. Schimmelpfennig, P. Neograd and L. Seijo, *Comput. Mater. Sci.*, 2003, **28**, 222.
12 D. Andrae, U. Haeussermann, M. Dolg, H. Stoll and H. Preuss, *Theor. Chim. Acta*, 1990, **77**, 123.
13 K. Pierloot, B. Dumez, P. O. Widmark and B. O. Roos, *Theor. Chim. Acta*, 1995, **90**, 87.
14 J. Full, C. Daniel and L. González, *Phys. Chem. Chem. Phys.*, 2003, **5**, 87.
15 (*a*) G. te Velde, F. M. Bickelhaupt, S. J. A. van Gisbergen, C. F. Guerra, E. J. Baerends, J. G. Snijders and T. Ziegler, *J. Comput. Chem.*, 2001, **22**, 931–967; (*b*) C. F. Guerra, J. G. Snijders, G. te Velde and E. J. Baerends, *Theor. Chem. Acc.*, 1998, **99**, 391; (*c*) ADF2007.01, SCM Theoretical Chemistry, Vrije Universiteit, Amsterdam, The Netherlands, 2000 http://www.scm.com.
16 E. J. Heller, *Acc. Chem. Res.*, 1981, **14**, 368.
17 C. C. Marston and G. G. Balint-Kurti, *J. Chem. Phys.*, 1989, **91**, 3571.
18 H. Tal-Ezer and R. Kosloff, *J. Chem. Phys.*, 1984, **81**, 3967.
19 B. Schmidt, WavePacket 4.2: A Program Package for Quantum-Mechanic Wavepacket Propagation, Free University Berlin, Berlin, 2005.
20 N. Balakrishman, C. Kalyanaraman and N. Sathyamurthy, *Phys. Rep.*, 1997, **280**, 79.